Intensity instabilities of semiconductor lasers under current modulation, external light injection, and delayed feedback

Joachim Sacher, Dieter Baums,* Peter Panknin, Wolfgang Elsässer, and Ernst O. Göbel
Fachbereich Physik der Philipps-Universität Marburg, Renthof 5, D-3550 Marburg, Federal Republic of Germany
(Received 29 April 1991; revised manuscript received 27 September 1991)

We investigate the occurrence of instabilities related to possible transitions to chaos in specific configurations based on semiconductor lasers. Various scenarios, such as period doubling, frequency locking, quasiperiodicity, and intermittency, are observed experimentally as functions of the control parameters. These are, respectively, the current modulation, external light injection, and delayed feedback. The experimental findings are described and discussed on the basis of semiconductor-laser rate equations.

PACS number(s): 42.50.Tj, 05.45.+b, 42.55.Px, 42.60.Fc

I. INTRODUCTION

Nonlinear dynamics and chaotic behavior have been studied recently in many systems belonging to different areas like biology, chemistry, or physics. The interesting aspect of these studies is the search for universality in the behavior of nonlinear systems and their transitions to chaos. Three universal transition routes from regular to chaotic motion have been observed so far in many different systems: the period-doubling (Feigenbaum) route, the intermittency (Pomeau-Manneville) route, and the quasiperiodic (Ruelle-Takens-Newhouse) route [1,2].

The period-doubling route refers to a successive series of period-doubling bifurcations that occur while changing a control parameter [3,4]. A transition to chaos takes place after an infinite number of doublings follow each other with a closer spacing. The intermittency route is characterized by an increasing number of short, irregular bursts, interrupting the nearly regular (laminar) motion. While varying a control parameter, the mean distance between these bursts changes. There are three different types of intermittency that can be distinguished by the statistics of the time intervals between the bursts. Type-I intermittency is associated with an inverse tangent bifurcation, type II with a Hopf bifurcation, and type III with a period-doubling bifurcation [2]. The quasiperiodic route corresponds to a series of Hopf bifurcations generating a new eigenfrequency each time one changes a control parameter [5]. The first Hopf bifurcation generates a limit cycle (periodic motion) in phase space emerging from a fixed-point (constant) solution. After the second Hopf bifurcation the motion of the system in phase space takes place on a two-dimensional torus allowing periodic as well as quasiperiodic behavior. The third Hopf bifurcation finally gives rise to the occurrence of deterministic chaos.

Nonlinear dynamics and chaotic behavior in laser systems have been investigated since the late 1970s [6]. All three universal transitions to chaos have been found in some gas laser systems, with the control parameters being pressure, wavelength tuning, and discharge current [7]. In contrast to these gas lasers, a solitary single-mode semiconductor laser cannot show chaotic behavior because it is fully described by two independent quantities only: the electric field and the carrier density. Therefore, semiconductor lasers can only show coupled light-carrier density oscillations, the relaxation oscillations. However, adding an additional degree of freedom allows the occurrence of chaotic instabilities. There are several possibilities to generate such additional degrees of freedom [8]. Some of them are mentioned in the present paper and three of them, also relevant for practical applications, will be discussed in detail.

This paper is structured as follows. In Sec. II we discuss the semiconductor-laser rate equations with respect to the possibilities of observing chaotic scenarios. The corresponding experimental setups are described in Sec. III. In Sec. IV we report frequency locking in terms of the Farey tree and the observation of the devil's staircase in a system consisting of an antireflection-coated semiconductor laser in an external resonator configuration with additional current modulation. Beginning with the recently published [9] observation of the devil's staircase in this system, we present here a detailed investigation of the Arnold tongues as a function of the modulation current. In Sec. V, the behavior of a semiconductor laser under external light injection is numerically simulated. In particular, the specific properties of semiconductor lasers are discussed with respect to the possibility of observing transitions to chaos. The theoretical predictions are compared to experimental observations. In Sec. VI, we report an intermittent transition between regular and irregular emission behavior in the coherence collapse of a semiconductor laser with delayed feedback. Recently published [10] experimental observations are confirmed by the comparison with numerical simulations. Section VII, finally, will summarize our present results and give some conclusions.

II. THEORETICAL BACKGROUND

The semiconductor-laser rate equations for a single-mode laser, as obtained in a semiclassical description by combining Schrödinger's equation with Maxwell's equa-

tions, read [11]

$$\frac{d\mathcal{E}}{dt}=-(i\omega_E+\gamma_E)\mathcal{E}-igP\ , \tag{2.1}$$

$$\frac{dP}{dt}=-(i\omega_P+\gamma_P)P+g\mathcal{E}N\ , \tag{2.2}$$

$$\frac{dN}{dt}=J-\gamma_N N+(2iPg\mathcal{E}^*-2iP^*g\mathcal{E})\ , \tag{2.3}$$

where the quantities have the following meanings: $\mathcal{E}$ is electric field strength, P the macroscopic polarization, N the inversion density, ω_E the oscillation frequency of the electric field strength, γ_E the photon decay rate, ω_P the oscillation frequency of the macroscopic polarization, γ_P the polarization decay rate, g the optical gain coefficient, and γ_N the inversion decay rate. Different types of lasers can be classified according to the values of the damping constants γ_E, γ_P, γ_N [12]. For class C lasers (e.g., far-infrared lasers) all three damping constants are of equal magnitude, and the laser has to be described by the full set of equations. As shown first by Haken [13], chaos can be expected for this type of laser analogous to the case discussed by Lorenz in the context of atmospheric turbulence [14]. In the case of class B lasers [12] (ruby, Nd:YAG, CO_2 and semiconductor lasers), the damping constant of the polarization γ_P is at least one order of magnitude larger than the other two damping constants γ_E and γ_N, which are comparable to each other. Therefore the polarization P can be eliminated adiabatically [15], and the system is fully described by the rate equations for the electric field $\mathcal{E}$ and the carrier density N,

$$\frac{d\mathcal{E}}{dt}=\{i\omega(N)+\tfrac{1}{2}[G(N)-\Gamma_E]\}\mathcal{E}\ , \tag{2.4}$$

$$\frac{dN}{dt}=J-\gamma_N N-G(N)|\mathcal{E}|^2\ , \tag{2.5}$$

where $\omega(N)$ and $G(N)$ are functions of the microscopic constants ω_E, ω_P, γ_P, and g. Furthermore, we have set $\Gamma_E=2\gamma_E$. Class B lasers can only show coupled electric field–carrier density oscillations, the relaxation oscillations. Finally, in class A lasers (He-Ne, Ar^+, and dye lasers), the inversion N can be eliminated adiabatically as well, because the damping constant γ_N is considerably larger than γ_E. Therefore, these systems have a fixed-point solution only.

Now, we want to continue with the semiconductor laser as an example of a class B laser. With respect to the investigation of laser instabilities and chaos, it is of great advantage that in particular the optical properties of solitary semiconductor-laser diodes have been investigated in great detail during recent years and are fairly well understood and described [16]. As already mentioned, the rate equations of the semiconductor laser predict stable behavior, and we have to add at least one additional degree of freedom to allow the occurrence of output instabilities and chaos. There are several possibilities to accomplish this.

The easiest one is to modulate the injection current periodically with a modulation frequency $\omega_{\rm mod}$. The pumping term J in Eq. (2.5) then has to be replaced by $J_{\rm dc}+J_{\rm ac}\cos\varphi(t)$, where $\varphi(t)$ is defined by

$$\frac{d\varphi}{dt}=\omega_{\rm mod}\ . \tag{2.6}$$

The rate equations (2.4) and (2.5) now read

$$\frac{d\mathcal{E}}{dt}=\{i\omega(N)+\tfrac{1}{2}[G(N)-\Gamma_E]\}\mathcal{E}\ , \tag{2.7}$$

$$\frac{dN}{dt}=J_{\rm dc}+J_{\rm ac}\cos\varphi-\gamma_N N-G(N)|\mathcal{E}|^2\ . \tag{2.8}$$

An analysis of these equations shows that for modulation frequencies $\omega_{\rm mod}$ above the relaxation oscillation frequency of a solitary laser diode, period doubling takes place. With further increase of the modulation frequency $\omega_{\rm mod}$ a period-doubling route to chaos is predicted [17,18]. In Sec. IV investigations of the external-cavity semiconductor laser with modulation frequencies comparable to the inverse resonator round-trip time will be discussed.

A second possibility to add an additional degree of freedom is to inject coherent light of frequency $\omega_0+\Delta\omega$, with $\Delta\omega$ typically some GHz. An additional electric field term $\mathcal{E}_1(t)$ then has to be added to the right-hand side of Eq. (2.4) to describe this configuration [19],

$$\mathcal{E}_1(t)=\kappa E_{\rm inj}\exp[i(\omega_0+\Delta\omega)t]\ . \tag{2.9}$$

The modified rate equations (2.4) and (2.5) are now

$$\frac{d\mathcal{E}}{dt}=\{i\omega(N)+\tfrac{1}{2}[G(N)-\Gamma_E]\}\mathcal{E}(t)+\mathcal{E}_1(t)\ , \tag{2.10}$$

$$\frac{dN}{dt}=J-\gamma_N N-G(N)|\mathcal{E}|^2\ . \tag{2.11}$$

Analysis of these rate equations shows [20] that with increasing difference frequency $\Delta\omega$ up to the relaxation oscillation frequency several period-doubling sequences and a transition to chaos will take place.

Finally, we want to discuss the coupled-cavity configuration, which also shows intrinsically unstable regimes. This configuration actually is of great practical relevance since coupled cavities are frequently employed, e.g., for linewidth reduction of semiconductor lasers. Furthermore, spurious feedback, as it occurs when coupling a laser diode to a fiber or in audio disc systems, corresponds also to the situation considered here. The coupled-cavity configuration can be considered as a delayed feedback of laser emission, back into the active region of the laser. Therefore in Eq. (2.4) a term $\mathcal{E}_1(t)$ describing the light that is coupled back into the laser has to be added. In this case $\mathcal{E}_1(t)$ is a function of the laser light $\mathcal{E}(t)$ delayed by the time τ corresponding to the round-trip time in the external resonator [21],

$$\mathcal{E}_1(t)=\kappa\mathcal{E}(t-\tau)\ . \tag{2.12}$$

From a mathematical point of view the system now becomes infinite dimensional due to the time delay τ in the external resonator. Formally, a description by the rate equation system (2.10) and (2.11) is still valid; however, the different meaning of $\mathcal{E}_1(t)$ given by Eq. (2.12) has to be considered. In principle, there are two possibilities to observe characteristic instabilities and deterministic

chaos. The first is to increase the intensity of the feedback light of the external resonator, i.e., the coupling of the external resonator to the laser diode. In this case a quasiperiodic transition route to chaos occurs [22,23]. The second possibility that we want to discuss in this paper is to keep the feedback rate at a high level and to increase the injection current. Then an intermittency route to chaos takes place [10].

In the following, we want to present the mathematical formalism to work with the rate equation system (2.10) and (2.4). First, we split the electric field into amplitude and phase using the following ansatz:

$$\mathcal{E}(t)=E(t)\exp[i\omega_0 t+i\phi(t)] \ . \tag{2.13}$$

We then obtain a rate equation for the amplitude $E(t)$ and phase $\phi(t)$ of the electric field $\mathcal{E}(t)$. Furthermore, we linearize the gain function $G(N)$ and the eigenfrequency $\omega(N)$ around the transparency value $N_{\rm LD}$ of the carrier density of the free-running semiconductor laser and consider the saturation of the gain function $G(N)$ at high light intensities:

$$G(N)=G_N(N-N_{\rm LD})=G_N\Delta N \ , \tag{2.14}$$

$$\omega(N)=\omega_0+\omega_N(N-N_{\rm LD})=\omega_0-\tfrac{1}{2}\alpha G_N\Delta N \ , \tag{2.15}$$

with

$$\alpha=-2\frac{\omega_N}{G_N} \ . \tag{2.16}$$

The linewidth enhancement parameter α [24] describes the coupling between the optical gain function and the refractive index of the laser material. The change in refractive index directly causes a change of the eigenfrequency of the semiconductor laser. More generally, the α parameter can be expressed by the nonlinear susceptibility [25] of the semiconductor-laser material,

$$\alpha=-\frac{d[\mathrm{Re}\chi(N)]/dN}{d[\mathrm{Im}\chi(N)]/dN} \ , \tag{2.17}$$

where the real part of the nonlinear susceptibility $\mathrm{Re}[\chi(N)]$ is proportional to the refractive index and the imaginary part $\mathrm{Im}[\chi(N)]$ is proportional to the optical gain function $G(N)$.

The gain saturation parameter ϵ accounts for the saturation of the optical gain function at high light intensities. The ansatz

$$G_N=G_N(|E(t)|^2)=\frac{G_{N0}}{1+\epsilon|E(t)|^2} \tag{2.18}$$

describes phenomenologically the experimentally observed saturation [26] of the differential gain $G_N(|E(t)|^2)$. If the light intensity dependence of the refractive index is ignored, this results in an intensity-dependent α parameter [27],

$$\begin{aligned}\alpha=\alpha(|E(t)|^2)&=-2\frac{\omega_N}{G_N(|E(t)|^2)}\\&=-2\frac{\omega_N}{G_{N0}}[1+\epsilon|E(t)|^2]\\&=+\alpha_0[1+\epsilon|E(t)|^2] \ .\end{aligned} \tag{2.19}$$

With these definitions (2.18) and (2.19) for α and ϵ and the linearized equations (2.14) and (2.15), we obtain the following expressions for $G(N)$ and $\omega(N)$:

$$G(N)=\frac{G_{N0}\Delta N}{1+\epsilon|E(t)|^2} \ , \tag{2.20}$$

$$\omega(N)=\omega_0-\tfrac{1}{2}\alpha_0 G_{N0}\Delta N \ . \tag{2.21}$$

Substituting Eqs. (2.13), (2.20), and (2.21) into Eqs. (2.10) and (2.11), we obtain three coupled rate equations describing the amplitude $E(t)$ and phase $\phi(t)$ of the electric field and the carrier density $N(t)$,

$$\frac{dE}{dt}=\frac{1}{2}\left[\frac{G_{N0}\Delta N}{1+\epsilon|E(t)|^2}-\Gamma_E\right]E(t)+E_1(t)\cos\Delta_1(t) \ , \tag{2.22}$$

$$\frac{d\phi}{dt}=-\tfrac{1}{2}\alpha_0 G_{N0}\Delta N(t)-\frac{E_1(t)}{E(t)}\sin\Delta_1(t) \ , \tag{2.23}$$

$$\frac{dN}{dt}=J-\gamma_N N-\frac{G_{N0}\Delta N}{1+\epsilon|E(t)|^2}|E(t)|^2 \ . \tag{2.24}$$

In the injection case, $E_1(t)$ and $\Delta_1(t)$ have the following meanings:

$$E_1(t)=\kappa E_{\rm inj} \ , \tag{2.25}$$

$$\Delta_1(t)=(\Delta\omega)t+\phi(t) \ . \tag{2.26}$$

In the feedback case, $E_1(t)$ and $\Delta_1(t)$ are given by

$$E_1(t)=\kappa E(t-\tau) \ , \tag{2.27}$$

$$\Delta_1(t)=\omega_0\tau+\phi(t)-\phi(t-\tau) \ . \tag{2.28}$$

We now describe the corresponding experimental setups before we discuss the experimental findings in Secs. IV, V, and VI in detail.

III. EXPERIMENTAL SETUP

For all experiments we used temperature-stabilized GaAs/$Ga_{1-x}Al_xAs$ channeled substrate planar (CSP) semiconductor-laser diodes (Hitachi HLP1400, emitting in the spectral regime of 830 nm) in three different experimental setups that are depicted schematically in Fig. 1.

In the configuration corresponding to the setup of Sec. IV, we use an external cavity configuration [Fig. 1(a)]. The laser diode is single-facet antireflection- (AR) coated ($R<0.001$), and the external cavity consists of a collimating microscope objective and a high-reflecting dielectric mirror ($R>0.98$). The injection current driving the laser diode consists of a modulation current at a frequency $f_{\rm mod}$ superimposed onto the dc current.

For the experiments discussed in Sec. V, we use a dc-

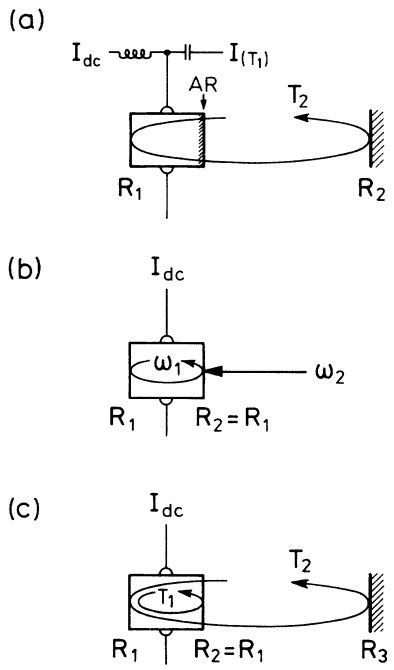

FIG. 1. Sketch of three model systems for the investigations of instabilities in semiconductor lasers: (a) the semiconductor laser with current modulation, (b) the semiconductor laser with external light injection, (c) the semiconductor laser with delayed feedback.

driven, uncoated semiconductor laser (pump laser), where the light of a second semiconductor laser (probe laser) is focused into the active region of the pump laser [Fig. 1(b)]. The two lasers are separated optically from each other using a Faraday rotator.

In the experimental configuration corresponding to Sec. VI, we use a coupled-cavity configuration that is similar to the setup of Sec. IV [Fig. 1(c)]. However, different from the configuration of Sec. IV, the laser

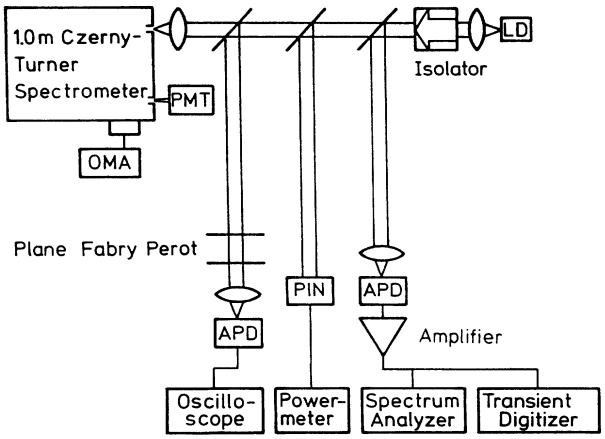

FIG. 2. Detection part of the experimental setup. The laser diode (LD) represents three types of experiments depicted in Figs. 1(a)–1(c). (PMT photomultiplier, OMA optical multichannel analyzer, APD avalanche photodiode, and PIN *p-i-n* photodiode.)

diode is dc driven, and the laser facets remain uncoated.

Figure 2 depicts the detection part of the experiment setup. The laser diode (LD) represents the three types of experiments shown in Fig. 1. The emitted light emerging from the laser diode is analyzed in the time, frequency, and spectral domain with respect to instabilities in the three types of experiments. The optical spectrum of the laser diode is measured using a 1-m Czerny-Turner grating monochromator and a scanning plane Fabry-Pérot interferometer. The time-averaged laser light intensity is measured by a slow *p-i-n* diode. The fluctuations of the laser intensity are detected employing a fast avalanche photodiode (APD, rise time ≤ 100 ps). Its electrical signal is amplified and then analyzed in the frequency and time domain using a rf spectrum analyzer and a transient digitizer (bandwidth = 600 MHz), respectively.

IV. THE SEMICONDUCTOR LASER WITH MODULATION OF THE INJECTION CURRENT

In this section we report on the emission behavior of a current modulated semiconductor laser. In the case of current modulation two cases can be distinguished: (1) The modulation frequency is of the same order or higher than the relaxation oscillation frequency. Then a period-doubling route to chaos is predicted on the basis of the rate equations [17]. (2) The modulation frequency is either of the order of the round-trip frequency of the laser photons within the resonator or amounts to a rational fraction p/q of the round-trip frequency. In this case frequency locking following the hierarchy of the Farey tree and quasiperiodicity is expected and has been observed [28], as will be discussed. For practical reasons the experiments are performed with an external cavity of length L; to avoid coupled-cavity effects (see Sec. VI), one facet of the semiconductor laser has been antireflection coated with high quality. The experimental setup is depicted schematically in Fig. 1(a) and fully described in Sec. III. This system is characterized by two frequencies: the modulation frequency $f_{\rm mod}$ and the inverse external resonator round-trip time $f_{\rm res}=c/2L$. It should be noted that this configuration with $f_{\rm mod}/f_{\rm res}=p/q=1$, i.e., the modulation frequency corresponds exactly to the round-trip frequency, is commonly employed for short optical pulse generation with semiconductor lasers (active or synchronous mode locking), resulting in the generation of a periodic pulse train with pulse widths in the 10 ps range.

Large detuning of one of the frequencies with respect to the other corresponds to trajectories in phase space lying on a two-dimensional torus. On such a two-dimensional torus there are two possibilities for the adjustment of the frequencies. They can be held at a rational ratio $f_{\rm mod}/f_{\rm res}=p/q$ which gives a closed curve on the torus, or the ratio can be an irrational value resulting in a never-closing (never-repeating) trajectory.

These two possibilities can be clearly observed experimentally using the time-resolved detection system consisting of the APD and the transient digitizer of Fig. 2. Experimental results are shown in Figs. 3(a) and 3(b) for two typical cases. In the first case ($f_{\rm mod}/f_{\rm res}=\frac{2}{5}$) the pulse train repeats after five pulses with different sizes

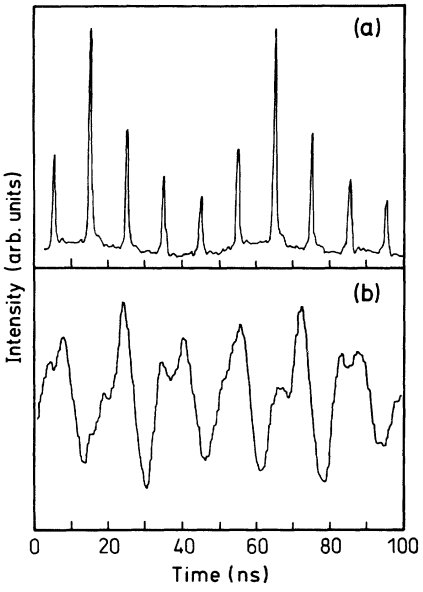

FIG. 3. (a) Frequency-locked output of the external cavity laser with modulation when the frequency ratio is chosen to be $f_{\rm mod}/f_{\rm res}=\frac{2}{5}$. (b) Quasiperiodic output of the modulated external cavity laser when the frequency ratio is set to the golden-mean value $\sigma_g=0.618\,03\ldots$.

[Fig. 3(a)], while for $f_{\rm mod}/f_{\rm res}=0.618\,03\ldots$, which is close to the golden mean $(\sqrt{5}-1)/2$, no periodicity in the light output could be found [Fig. 3(b)]. This behavior (termed frequency locking in nonlinear dynamics [29]) is modeled by a very simple one-dimensional map, the standard circle map

$$\theta_{n+1}=f(\theta_n)=\theta_n+\Omega-\frac{K}{2\pi}\sin 2\pi\theta_n\ , \tag{4.1}$$

which is the discrete version of the Adler equation derived for the frequency locking of oscillations [30] and mode-locked lasers [31,28].

This map predicts frequency locking at every rational number $\Omega=p/q$ (corresponding to our frequency ratio), ordered according to the hierarchy of a Farey tree with a locking range of finite width. The light output is quasiperiodic for Ω between these locked states. The widths of the locking ranges increase with increasing nonlinearity K until, at $K=1$, complete frequency locking is achieved. Then all the locking ranges plotted against the frequency range form a complete devil's staircase with a dimension of 0.87. For larger K, chaos becomes possible. The frequency-locking behavior can also be calculated from the rate equations (2.6)–(2.8), as has been shown in Refs. [32] and [33].

The predictions according to the one-dimensional circle map have been checked for the present system [9]. Frequency locking has been observed down to very low levels in the Farey tree. The observed ratios are shown in Fig. 4. The corresponding locking ranges are plotted against the modulation frequency in Fig. 5. The resulting staircase (the upper curve in Fig. 5) is in very close accordance with the one calculated according to Eq. (4.1) [5].

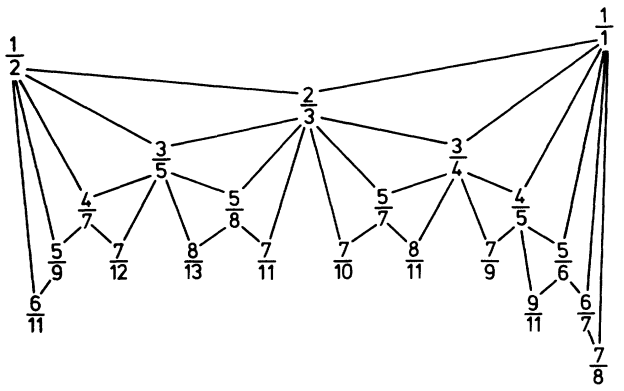

FIG. 4. Observed frequency-locking ratios in the interval $\frac{1}{2}\le p/q\le\frac{1}{1}$ ordered according to the Farey-Tree construction.

The evaluation of the fractal dimension following Ref. [34] yields $D=0.89$, which is very close to the value of $D=0.87$, supporting the hypothesis that the modulated semiconductor laser with an external resonator belongs to the universal class of systems exhibiting the quasiperiodic route to chaos. In addition, we have plotted in Fig. 5 the averaged power of the optically emitted pulse trains (lower curve in Fig. 5). We observe a more or less pronounced peak whenever a frequency-locked state occurs. This indicates that the frequency-locked states exhibit some resonance behavior with regard to the output power. Yet, compared to the fundamental locking at $p/q=1$, the other resonances for $p/q<1$ are much weaker.

As already mentioned, the quasiperiodic and frequency-locked behavior is predicted by Eq. (4.1). However, this mathematical map does not predict under which circumstances chaos will definitely be observed. Most probably, a transition to chaos takes place by increasing K at the golden mean winding number. For our system it seems reasonable to relate the modulation am-

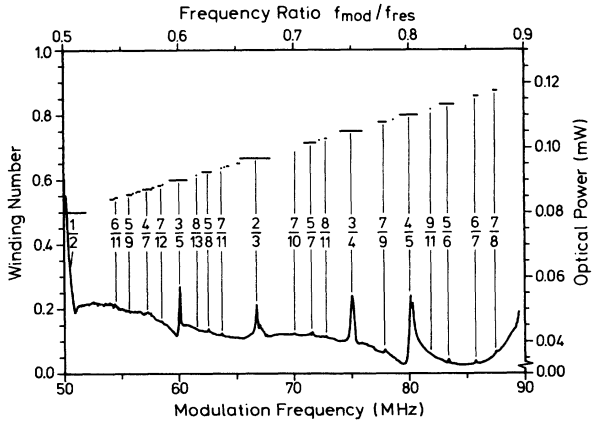

FIG. 5. Ratio of the response frequency to the driving modulation frequency (winding number; left scale, upper curve) and averaged output power (right scale, lower curve) as a function of the modulation frequency. The modulation amplitude was kept constant and the resonator frequency $f_{\rm res}$ amounted to 100 MHz.

plitude of the driving current to the nonlinearity parameter K. Experimentally, however, we observe for the modulated semiconductor laser a transition from a quasiperiodic output to gain switching as the modulation amplitude J_{ac} is increased. In the gain-switching regime, the laser diode is switched on and off by the large modulation current, and the feedback of the resonator does not affect the behavior at all. This is due to the fact that the antireflection coating is not perfect, and thus for high-modulation amplitudes lasing occurs within the solitary laser diode. The different regimes of operation are shown in Fig. 6. The shaded areas are the frequency-locked states [such as Fig. 3(a)] with respect to the modulation power. The unshaded region in between refers to quasiperiodic output of light intensity [Fig. 3(b)]. On the bottom of the graph these regimes are limited by cw operation for the case, where the modulation is too weak to have a strong influence on the output behavior. On the top of the graph the cross-shaded region represents the regime of gain switching. The delayed feedback by the external resonator mirror then acts only as a small disturbance to the solitary laser diode which is switched on and off. In that case the external resonator round-trip frequency is suppressed instead of creating chaotic output by nonlinear competition between the two frequencies.

It should be noted that the actual form of the frequency-locked states with the modulation amplitude as a control parameter does not correspond to the behavior predicted by Eq. (4.1). Instead of observing the typical Arnold tongues with an overlap at $K=1$ and a possible transition to chaos, we find a decrease of the width of the Arnold tongues and a transition to a new, different ordered state as the modulation amplitude is raised. Even though this behavior may be attributed to the nonperfect antireflection coating of the laser facet, it might be of principle interest that the modulated semiconductor laser within a certain regime of the modulation amplitude can be described according to the one-dimensional circle map; whereas for other regimes this description obviously fails.

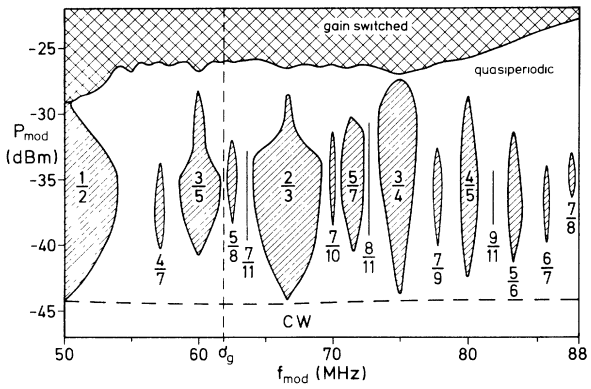

FIG. 6. Experimentally determined operation regimes (gain switching, quasiperiodicity, frequency locking, and cw operation) of the modulated external cavity semiconductor laser as a function of the modulation frequency and rf modulation power. The shaded areas are the frequency-locked states (in nonlinear dynamics referred to as the Arnold tongues). The space in between corresponds to quasiperiodic emission behavior. For small values of modulation power the laser operates in a cw mode (bottom), whereas for the case of high modulation amplitude (top, cross-shaded area) the laser operates in a gain-switched mode. In all cases f_{res} is equal to 100 MHz.

V. THE SEMICONDUCTOR LASER WITH AN INJECTED SIGNAL

In this section we present results of the irregular emission behavior of a semiconductor laser with injected coherent light. The experimental setup is depicted in Fig. 1(b) and described in Sec. III. The injection of coherent light into a semiconductor laser is commonly referred to as four-wave-mixing (FWM) [35] or injection locking [36], depending on the experimental conditions [37]. FWM means the generation of new sideband frequencies due to the third-order nonlinear susceptibility $\chi^{(3)}$, which is very efficient in semiconductor lasers [38]. Injection locking refers to a complete phase locking between the laser light and the injected light [36]. For small detuning frequencies between the laser light frequency and the frequency of the injected light, injection locking appears, whereas for large detunings FWM is observed [37]. Both processes reflect possible solutions of the rate equations [Eqs. (2.22)–(2.24) together with (2.25) and (2.26)]. Furthermore, on the basis of these rate equations, it can be concluded that the semiconductor laser with external coherent light injection should exhibit chaotic behavior, in principle. In the following, we present numerical simulations of the differential equation system and characterize these results by different methods with respect to possible chaotic emission behavior in the intermediate regime between the locking range and the region where FWM appears. Furthermore, we demonstrate the important influence of the linewidth enhancement parameter α and the gain saturation parameter ϵ on the dynamical behavior of this system. Then we report some preliminary experimental results indicating that chaotic instabilities via a period-doubling route in fact may occur in this intermediate regime.

Equations (2.22)–(2.24) together with (2.25) and (2.26) have been integrated numerically, and subsequently the time-dependent complex electric field $\mathcal{E}$ has been Fourier transformed. Figure 7 shows the resulting intensity spectra for different detuning frequencies $\Delta\omega$ between the original laser field $\mathcal{E}_0$ and the injected field $\mathcal{E}_{inj}$ assuming $E_{inj}=\frac{1}{60}E_0$ for the ratio of the field amplitudes. In Fig. 7(a) a typical spectrum with relaxation oscillations and multiples is depicted. The relaxation oscillations become enhanced due to the injected light. A decrease in the detuning $\Delta\omega$ results in the occurrence of new frequencies at a half-spacing [Fig. 7(b)]. A further decrease in $\Delta\omega$ results in the occurrence of additional frequencies [Fig. 7(c)], and the spectrum broadens considerably, until a broad noise spectrum is observed [Figs. 7(d) and 7(e)] (note that the FWM regime is not depicted in this figure). It is worth pointing out that this behavior occurs without inclusion of noise sources in the rate equations. It seems that the system under the conditions corresponding to Figs. 7(d) and 7(e) has become chaotic; however, this has

to be analyzed and proven, quantitatively. A definite conclusion is not possible on the basis of the frequency spectrum only. We therefore have performed in addition a phase-space analysis in order to distinguish between periodic, quasiperiodic, and chaotic motion [2]. This analysis can be performed by investigations of two-dimensional projections (Poincaré cuts) of the three-dimensional phase space, which is spanned by the inversion and either modulus and phase or real and imaginary parts of the field. Instead of investigating the complete three-dimensional trajectory, only the intersection points of the trajectory, common with an arbitrarily two-dimensional plane in phase space, are chosen. This manifold of points contains the same topological properties as the original phase space. Finally, this procedure is followed by a subsequent dimensional analysis. A typical Poincaré plot is shown in Fig. 8, where we have plotted the real and imaginary parts of the complex electric field $\mathcal{E}$ for the plane defined by the transparency value N_{LD} of the carrier concentration. The picture consists of 35 000 data points. A periodic or quasiperiodic as well as a white-noise-determined behavior can be excluded definitely on the basis of this figure. Quasiperiodic behavior would show up as a repetitive cycle after one round-trip time, while in contrast white noise would correspond to a continuous distribution of the points. Instead, structures typical for the occurrence of chaos are obvious: Regions that are frequently occupied are well separated by pronounced windows, reflecting the fractal dimension of the phase-space trajectory [39]. Finally, the dimensional analysis allows quantitative proof [1]. The dimension of a quasiperiodic trajectory is equal to the number of incommensurate frequencies, i.e., a natural number. A chaotic movement is distinguished by a rational dimension, larger than two. From an analysis of the simulated data of Fig. 8 values for the information and correlation dimension [1,40,41] of $D_1=2.91$ and $D_2=2.66$ are obtained, respectively. These dimensions are rational numbers and a quasiperiodic and white-noise-dominated behavior can thus be definitely excluded.

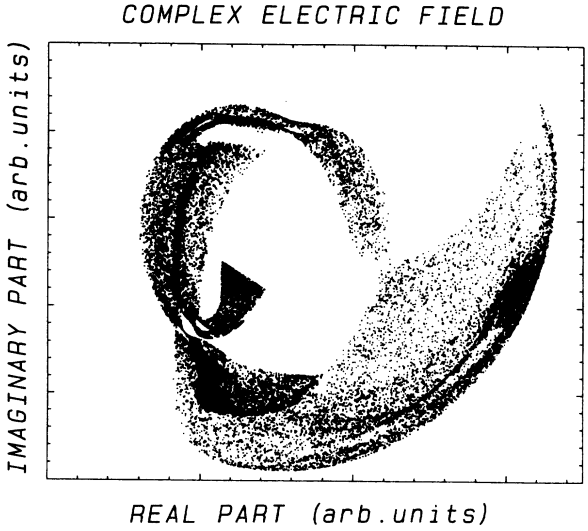

FIG. 8. Poincaré plot constructed from the simulated data as depicted in Fig. 7(e). Plotted are the intersection points of the trajectories for the plane of the complex electric field $\mathcal{E}$ defined by the transparency value N_{LD} of the carrier density.

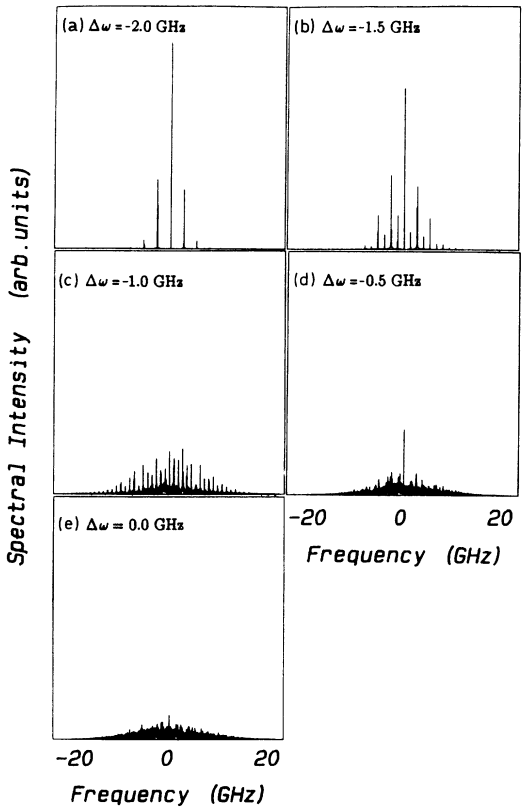

FIG. 7. Simulated spectra for five different detuning frequencies $\Delta\omega$: (a) $\Delta\omega=-2.0$ GHz, (b) $\Delta\omega=-1.5$ GHz, (c) $\Delta\omega=-1.0$ GHz, (d) $\Delta\omega=-0.5$ GHz, and (e) $\Delta\omega=0.0$ GHz. The frequency at ± 2.3 GHz (a) corresponds to the relaxation oscillations of the laser.

Consequently, chaos should be initiated by light injection into the cavity of a semiconductor laser. The remaining questions concern the respective scenario by which the transition occurs and the identification of the relevant control parameters. To answer these questions, bifurcation diagrams have been constructed from the time series of the electric field amplitude E. Figure 9 shows bifurcation diagrams with the detuning frequency $\Delta\omega$ [9(a)] and the injected electric field amplitude E_{inj} [9(b)] as the control parameter. E_{max} depicts the values of the maxima of the electric field amplitude E occurring in the respective time trace. The unit $\mathrm{cm}^{-3/2}$ of the electric field amplitude originates from the condition that the absolute square of the electric field strength $|\mathcal{E}|^2$ is equal to the photon density in the active region of the laser diode. The figure shows several period-doubling cascades separated by chaotic regimes. In addition, the bifurcation diagram shows an abrupt steplike behavior, e.g, for $\Delta\omega=1.7$ GHz in Fig. 9(a). This is consistent with a change in the value of the attractor. These sudden changes represent a so-called crisis of the attractor, according to Greborgi, Ott, and Yorke [42]. Crisis-induced

chaos can be understood as due to a collision of the chaotic attractor with a coexisting unstable fixed point, also present in the bifurcation diagram. Thus we conclude that the electric field amplitude E_{inj} as well as the detuning frequency $\Delta\omega$ can serve as a control parameter, and in both cases a period-doubling route to chaos is expected.

Before we report some preliminary experimental results, we want to discuss the influence of the specific semiconductor-laser properties that are reflected in high values for the linewidth enhancement parameter α and the gain saturation parameter ϵ. Figure 10 illustrates the important influence of the α parameter. The pumping term J is slightly different than in Fig. 8, otherwise the parameters are the same. We have plotted the maxima of the light intensity occurring in the respective time trace for values of α between $\alpha=0$ [Fig. 10(a)] and $\alpha=3$ [Fig. 10(d)] in steps of 1. The realistic value of $\alpha=4$ [25] is actually depicted in Fig. 11(a), where the influence of the ϵ parameter is discussed. For $\alpha=0$, the bifurcation diagram is symmetric with respect to zero detuning, and chaotic behavior is suppressed [Fig. 10(a)]. For an increasing α parameter [Figs. 10(a)–10(d)] the bifurcation diagram becomes asymmetric; the width of the locking regime becomes smaller and is shifted to negative frequencies. The shift of the locking range can be attributed to the induced change of the carrier density, which causes a change of the refractive index and finally results in a shift of the eigenfrequency $\omega(N)$ of the laser diode. This explains the strange behavior at first view that the chaotic emission behavior appears for zero detuning frequency. Furthermore, we have to note that the occurrence of chaos and instabilities is favored by a large value of the α parameter, which actually is the case for semiconductor lasers in contrast to other laser systems.

Next we discuss the influence of the gain saturation parameter ϵ on the nonlinear dynamics of the laser emission. In Fig. 11 we have plotted a series of bifurcation diagrams for different ϵ values. We have increased the value for ϵ from $\epsilon=0$ cm^3 [Fig. 11(a)] up to realistic values [43] between $\epsilon=5\times10^{-18}$ cm^3 [Fig. 11(c)] and $\epsilon=1\times10^{-17}$ cm^3 [Fig. 11(d)]. The calculated results show that an increase of ϵ tends to suppress the occurrence of instabilities. At high values of ϵ the width of the locking range increases, and the chaotic emission behavior is shifted to higher values of the amplitude of the

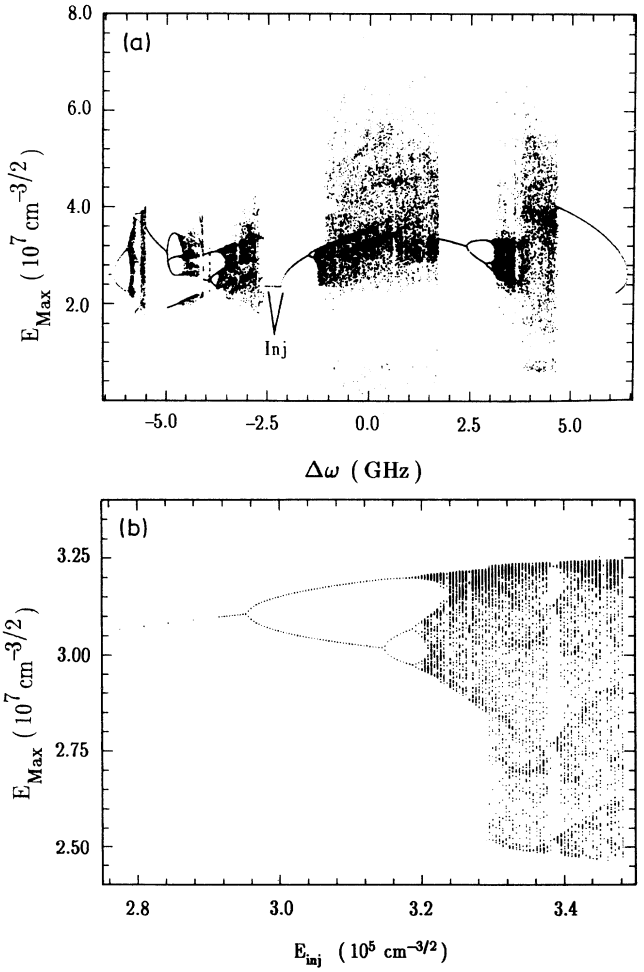

FIG. 9. Bifurcation diagrams with detuning frequency $\Delta\omega$ [(a) upper part] and the injected field amplitude E_{inj} [(b) lower part] as the control parameter, respectively. Plotted are the maxima of the electric field amplitude E occurring in the respective time trace. The locking range is indicated by inj. The values of α and ϵ are $\alpha=4$, $\epsilon=0$ cm^3.

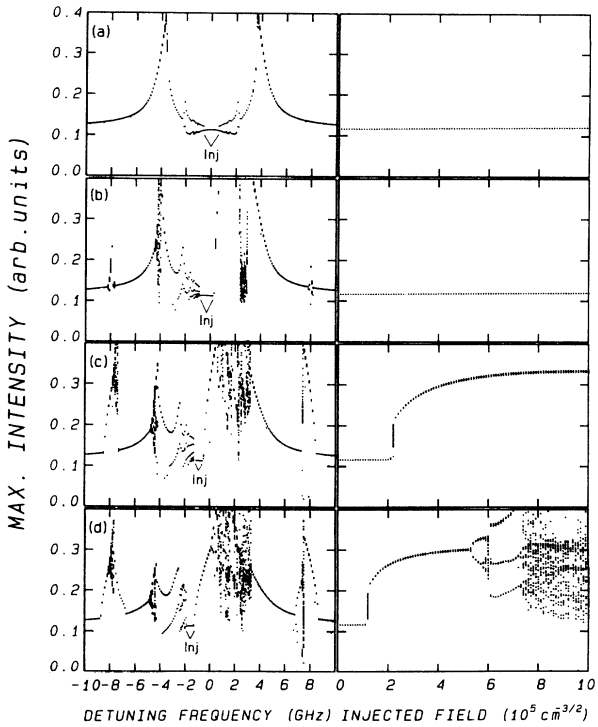

FIG. 10. Bifurcation diagrams with detuning frequency $\Delta\omega$ (left column, $E_{inj}=5\times10^5$ cm$^{-3/2}$) and the injected field amplitude E_{inj} (right column, $\Delta\omega=0.0$ GHz) as the control parameter, respectively. Plotted are the maxima of the light intensity occurring in the respective time trace. The locking range is indicated by inj. This figure demonstrates the influence of the α parameter [(a) $\alpha=0$; (b) $\alpha=1$; (c) $\alpha=2$; (d) $\alpha=3$]. The value of ϵ is $\epsilon=0$ cm^3.

injected light. Obviously, the effect of α and ϵ is opposite. Whereas increasing α tends to favor the occurrence of instabilities and chaos, increasing ϵ causes a damping of the system [18].

Experimentally, we have recently obtained an indication for the occurrence of instabilities via a period-doubling route. Figure 12 depicts an experimentally determined series of Fabry-Pérot spectra for four different values of the detuning frequency between the pump laser LD_1 and the probe laser LD_2. Plotted is the output density spectrum for different injection currents of one of the laser diodes, which corresponds to different detunings, since the emission frequency shifts with injection current. The free spectral range (FSR) in each part of Fig. 12 amounts to 30 GHz. In order to tune the emission frequency of the probe laser LD_2, we have changed its injection current I_2. Figure 12(a) corresponds to the case of injection locking. Note, however, that this does not necessarily correspond to $\Delta\omega=0$ of the free-running lasers. In Fig. 12(b) the detuning frequency between both lasers is increased, and the Fabry-Pérot spectrum shows a typical spectrum with injection-enhanced relaxation oscillations of pump laser LD_1. A further increase of the detuning frequency into the transition regime between the enhanced relaxation oscillations and the FWM regime causes a period doubling that results in the frequency signal in the middle between the frequencies corresponding to the pump laser LD_1 and probe laser LD_2 [Fig. 12(c)]. However, with a further increase of the detuning frequency, the signal corresponding to the period-doubled frequency disappears and a "normal" FWM spectrum is observed [Fig. 12(d)], which consists of the frequency of the pump laser LD_1, of the probe laser LD_2, and of the newly generated FWM signal on the right-hand side of LD_1.

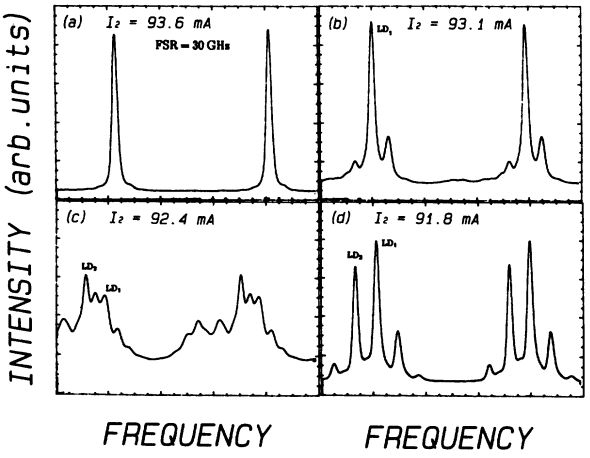

FIG. 12. Experimentally determined series of Fabry-Pérot spectra with increasing detuning frequency between the pump laser LD_1 and the probe laser LD_2: (a) injection locking between pump laser LD_1 and probe laser LD_2 (b) injection-enhanced relaxation oscillations, (c) period-doubled signal, (d) four-wave-mixing signal.

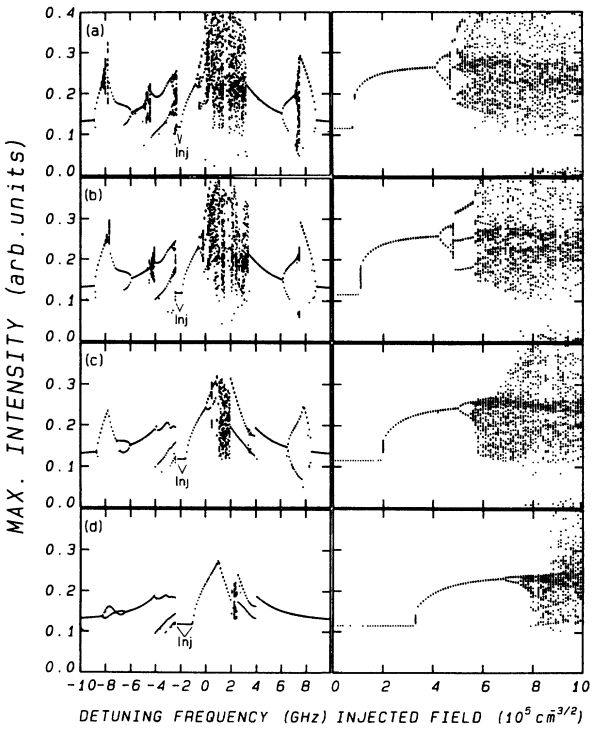

FIG. 11. Bifurcation diagrams with detuning frequency $\Delta\omega$ (left column, $E_{inj}=5\times10^5$ cm$^{-3/2}$) and the injected field amplitude E_{inj} (right column, $\Delta\omega=0.0$ GHz) as the control parameter, respectively. Plotted are the maxima of the light intensity occurring in the respective time trace. The locking range is indicated by inj. This figure demonstrates the influence of the ϵ parameter [(a) $\epsilon=0$ cm^3; (b) $\epsilon=1\times10^{-18}$ cm^3; (c) $\epsilon=5\times10^{-18}$ cm^3; (d) $\epsilon=1\times10^{-17}$ cm^3]. The value of α is $\alpha=4$.

These observations may give some preliminary indication on the occurrence of instabilities via the period-doubling route to chaos. However, it seems to be necessary to increase the intensity of the injected light up to much higher values to observe the predicted chaotic scenarios. On the other hand, it might be that the transition to chaos will be suppressed because of the high value of ϵ. However, it should also be pointed out once again that the numerical simulations have been performed without inclusion of any noise terms. Noise will cause a partial destruction of period-doubling sequences, and as a result, chaos may occur with less period doublings as theoretically predicted [44]. It has to be considered that experimentally a simple straightforward path in the complicated phase space of the system is difficult to realize. Consequently, the fact that a clear transition to chaos has not been observed so far may not be surprising. Further investigation of this system is required to give a full description of the system, especially with respect to the possibility of the occurrence of instabilities and chaos.

VI. THE SEMICONDUCTOR LASER WITH EXTERNAL FEEDBACK

The third topic we want to discuss in some detail is the irregular emission properties of the coupled-cavity configuration. The dynamics of instabilities in this system have been studied by several groups. Glas, Müller,

and Wallis [45] as well as Cho and Umeda [46] have found correlation dimensions of the emitted light intensity time series that indicate deterministic chaos under strong feedback conditions. Mukai and Otsuka [47] have reported the occurrence of subharmonic frequencies in the light intensity of an external cavity system with a tilted external mirror. Our group has found an intermittent generation of a regular oscillation with the tilting angle of the external cavity mirror as the control parameter [48]. Furthermore, we have found and characterized the appearance of intermittency in the transition region between regular and irregular emission behavior under the variation of injection current [10]. Recently, Mørk, Mark, and Tromborg have analyzed the route to chaos for the variation of the feedback level [22]. They have found a complex quasiperiodic transition to chaos. The appearance of this ultrafast optical chaos is accompanied by a dramatic increase of the spectral linewidth from some MHz to several GHz [49,50]. In contrast, for moderate levels of feedback the linewidth of the laser is reduced. The increase of the laser linewidth occurs above a critical value of the feedback level κ, which depends on the length of the external cavity [50,51]. The origin of this coherence collapse is the occurrence of a bistability between the state of minimal gain and the state of minimal linewidth [50,52]. In this section we present experimental data showing the occurrence of intermittency in the strong feedback case, and we compare the experimental results with numerical simulations of Eqs. (2.22)–(2.24) together with Eqs. (2.27) and (2.28).

The light power-injection current characteristics (*P-I* characteristic) of the solitary laser diode and the external cavity laser diode are shown in Fig. 13. The *P-I* characteristic is strictly linear above the laser threshold without external feedback. With feedback, the threshold current is reduced by 8%, which is within the regime where the coherence collapse occurs [51,53]. The *P-I* characteristic with external feedback exhibits a kink in the current regime corresponding to the threshold of the solitary laser diode. The power spectra of the emitted laser light at injection levels below and above the kink are depicted as insets in Fig. 13. The power spectrum for an injection current below the regime of the kink [inset (a)] exhibits a double-peak structure in the vicinity of the inverse external cavity round-trip time. The frequency f_e of the narrow, low-frequency peak is determined by the length L of the external cavity: $f_e \simeq c/2L$ (=352 MHz in the present case). The slightly broader peak, which is shifted by 36 MHz to higher frequencies with respect to the round-trip frequency f_e, is related to the relaxation oscillations of the solitary laser diode [54]. The upper inset (b) in Fig. 13 shows a typical power spectrum for an injection current in the region of the kink (point *b*). The width of the peaks in the region of the inverse external cavity round-trip time has dramatically increased, and a pronounced low-frequency noise occurs. This behavior is attributed to the occurrence of the coherence collapse [55]. Furthermore, it indicates an increase of the degrees of freedom reflecting the location of the system in phase space. The emission of the coupled-cavity laser in the regime of the coherence collapse is investigated in more de-

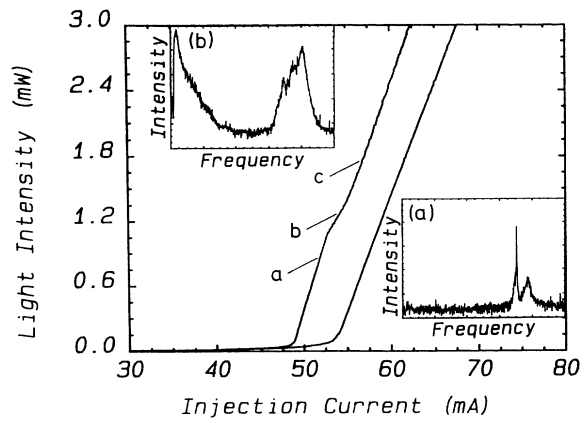

FIG. 13. Light power-injection current characteristics (*P-I* characteristic) of a semiconductor laser without optical feedback (right) and with optical feedback (left). The *P-I* characteristic with feedback exhibits a kink in the region of the threshold of the solitary laser. The lower inset (a) shows a typical power spectrum in the regime below the kink (point *a*). The upper inset (b) shows a corresponding power spectrum in the regime slightly above the kink (point *b*). The frequency scale of the insets ranges from 0 to 500 MHz, the intensity scale from −87 to −67 dB m.

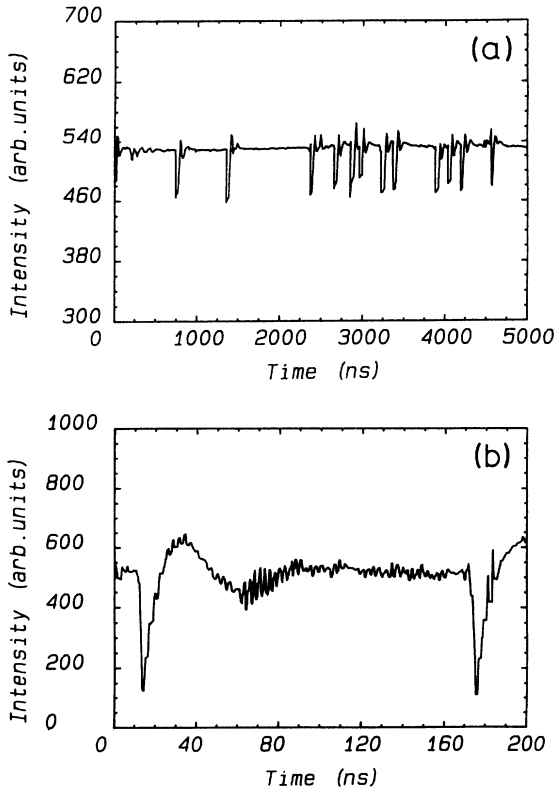

FIG. 14. Single-shot time traces of the light intensity for a current value slightly above the kink. (a) Long-time behavior: The light output shows statistically distributed break down events. (b) Detailed behavior on a short time scale: The light output breaks down and relaxes to the equilibrium value. The weaker, fast oscillation corresponds to the external cavity round-trip time.

tail by detecting the fluctuations of the laser light in the time domain using a transient digitizer. Figure 14 shows typical wave forms of the laser output for a current value in the intermediate region (cf. Fig. 13, point *b*) slightly above the kink on a long [Fig. 14(a)] and a short time scale [Fig. 14(b)]. The light intensity exhibits intermittent breakdown events with a characteristic statistical distribution and subsequent relaxation oscillations ($\tau_{\text{relax}} \simeq 40$ ns) to the equilibrium value. The frequency of the fast oscillating component ($\tau_e \simeq 2.8$ ns) in Fig. 14(b) corresponds to the external cavity round-trip frequency f_e. In this transition region between regularity (cf. Fig. 13, point *a*) and chaos (point *c*), the low-frequency noise is Fourier correlated to the rate of breakdown events. Recently, we have characterized this intermittent behavior as a time-inverted type-II intermittency by the statistical behavior of the breakdown events and by reconstructing a Poincaré plot [10]. Now, we want to compare the experimental behavior with numerical simulations of Eqs. (2.22)–(2.24) together with (2.27) and (2.28), in order to demonstrate that controlled chaotic behavior of a semiconductor laser is easily achieved with simple external control parameter variations that cause an increase in the degrees of freedom up to more than two. The parameters of Eqs. (2.22)–(2.24) and (2.27) and (2.28) (such as G_N, Γ_E, and γ) have been determined carefully by comparison of the stable solutions of Eqs. (2.22)–(2.24), (2.27), and (2.28) with the corresponding experimental data. In order to compare the numerical results for the time series of the emitted light intensity qualitatively with the experimentally obtained results, we have taken into account the finite bandwidth of our experimental equipment. For this reason, the simulated time series have been smoothed by a 1.5-ns time window. Figure 15 represents a typical simulated time evolution at the beginning of the unstable parameter region of the external cavity laser (cf. Fig. 13, point *b*). The calculated behavior of the light output exhibits irregular breakdown events of the light intensity and subsequent relaxation processes that are very similar to the experimentally determined temporal fluctuations of the light intensity (Fig. 14). For these operation conditions, realistic values of the gain saturation parameter ϵ [43] do not change the principle temporal behavior of the system. In order to continue the comparison between theory and experiment, we have calculated the power spectrum of the data corresponding to

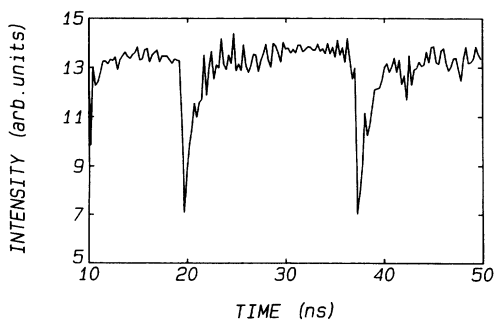

FIG. 15. Simulated time evolution of the light intensity under external feedback conditions according to Eqs. (2.22)–(2.26).

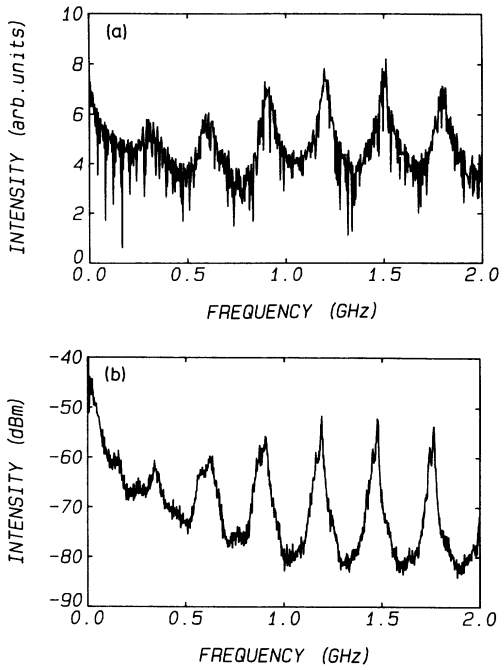

FIG. 16. (a) Power spectrum calculated from the simulated time evolution of the light intensity; (b) measured power spectrum of the light intensity fluctuations under external feedback conditions.

Fig. 15, which is shown in Fig. 16(a). Figure 16(b) depicts the corresponding experimental power spectrum. Both Fig. 16(a) and 16(b) show the typical broad spectra at the beat frequencies of the longitudinal external cavity modes and the low-frequency noise, which we have assigned to be characteristic for the occurrence of the coherence collapse.

To conclude this section we want to recall the discussions of Sec. II. We realize that the model describing the semiconductor laser in a feedback system incorporates an infinite number of degrees of freedom due to the delay term in Eqs. (2.22)–(2.24) together with (2.27) and (2.28). Therefore, instabilities and transitions to chaos have been found to be possible due to the dimensionality of this system.

VII. CONCLUSIONS AND SUMMARY

We have discussed and investigated different configurations based on semiconductor lasers, which—within certain regimes for the control parameter—show output instabilities and possible transitions to chaos. In particular we have considered (a) periodic modulation of the injection current, (b) external coherent light injection, and (c) the coupled-cavity semiconductor laser. The system (a) shows frequency locking and quasiperiodicity in accordance with the general features predicted by the one-dimensional circle map. Yet, a transition to chaos has not been observed so far, most likely due to experimental limitations. For case (b) we predict a period-doubling route to chaos, and finally, for the configuration (c) we observe a time-inverted type-II intermittency. The

experimental studies give preliminary indication for the correctness of the predictions. Apart from their applied relevance, our investigations demonstrate that at least some of the universal features of the dynamics of nonlinear systems can be conveniently studied with semiconductor lasers. In this respect, the specific properties of semiconductor lasers are not relevant. In other cases, however, e.g., for external coherent light injection, the specific properties of the semiconductor laser (high α parameter, high ϵ parameter) are of particular significance. Thus, the semiconductor-laser-based study of nonlinear dynamics combines aspects of material science and fundamental semiconductor physics with quantum optics and nonlinear dynamics. This is one of the reasons why we consider this area of research so exciting and promising for the future.

ACKNOWLEDGMENTS

We would like to thank S. Schmitt-Rink for a careful reading of the manuscript. This work has been supported by the Deutsche Forschungsgemeinschaft through the Sonderforschungsbereich 185 "Nichtlineare Dynamik."

*Present address: SEL–Alcatel Research Center, Lorenzstrasse 10, D-7000 Stuttgart, Germany.

[1] H. G. Schuster, *Deterministic Chaos* (VCH, Weinheim, 1988).
[2] P. Bergé, Y. Pomeau, and C. Vidal, *Order Within Chaos* (Hermann, Paris, 1984).
[3] S. Grossmann and S. Thomae, Z. Naturforsch. **32A**, 1353 (1977).
[4] M. J. Feigenbaum, J. Stat. Phys. **19**, 25 (1978).
[5] M. Jensen, P. Bak, and T. Bohr, Phys. Rev. Lett. **50**, 1637 (1983).
[6] See, e.g., R. G. Harrison, Contemp. Phys. **29**, 341 (1988); J. Opt. Soc. Am. B (special issue on laser instabilities) **5** (1989).
[7] See, e.g., F. T. Arecchi, R. Meucci, G. Puccioni, and J. Tredicce, Phys. Rev. Lett. **49**, 1217 (1982); C. O. Weiss, A. Godone, and A. Olafson, Phys. Rev. A **28**, 892 (1983); R. S. Gioggia and N. B. Abraham, Phys. Rev. Lett. **51**, 650 (1983).
[8] W. Elsässer, in *Festkörperprobleme* (Advances in Solid State Physics), edited by V. Rössler (Vieweg, Braunschweig, 1990), Vol. 30, p. 321.
[9] D. Baums, W. Elsässer, and E. O. Göbel, Phys. Rev. Lett. **63**, 105 (1989).
[10] J. Sacher, W. Elsässer, and E. O. Göbel, Phys. Rev. Lett. **63**, 2224 (1989).
[11] H. Haken, *Licht und Materie II* (BI-Wissenschaftsverlag, Zürich, 1981), Chap. 6.2.
[12] J. R. Tredicce, F. T. Arecchi, G. L. Lippi, and G. P. Puccioni, J. Opt. Soc. Am. B **2**, 173 (1985).
[13] H. Haken, Phys. Lett. **53A**, 77 (1975).
[14] E. N. Lorenz, J. Atmos. Sci. **20**, 130 (1963).
[15] H. Haken, *Advanced Synergetics* (Springer-Verlag, Berlin, 1983).
[16] G. P. Agrawal and N. K. Dutta, *Long-Wavelength Semiconductor Lasers* (Van Nostrand, New York, 1986).
[17] C.-H. Lee, T.-H. Hoon, and S.-Y. Shin, Appl. Phys. Lett. **46**, 95 (1985); L. Chausseau, E. Hemery, and J.-M. Lourtioz, *ibid.* **55**, 822 (1989).
[18] G. P. Agrawal, Appl. Phys. Lett. **49**, 1013 (1986).
[19] See, e.g., A. E. Siegman, *Lasers* (University Science Books, Mill Valley, CA, 1986).
[20] P. Panknin, Ph.D. thesis, Philipps—Universität Marburg, Germany, 1990.
[21] R. Lang and K. Kobayashi, IEEE J. Quantum Electron. **QE-16**, 347 (1980).
[22] J. Mørk, J. Mark, and B. Tromborg, Phys. Rev. Lett. **65**, 1999 (1990); J. Mørk, B. Tromborg, and J. Mark (unpublished).
[23] G. C. Dente, P. S. Durkin, K. A. Wilson, and C. E. Moeller, IEEE J. Quantum Electron. **QE-24**, 2441 (1988).
[24] C. H. Henry, IEEE J. Quantum Electron. **QE-18**, 259 (1982).
[25] M. Osiński and J. Buus, IEEE J. Quantum Electron. **QE-23**, 9 (1987).
[26] D. J. Chanin, J. Appl. Phys. **50**, 3858 (1979); J. E. Bowers, B. R. Hemenway, A. H. Gnauck, and D. P. Wilt, IEEE J. Quantum Electron. **QE-22**, 833 (1986); A. Tomita and A. Suzuki, *ibid.* **QE-27**, 1630 (1991).
[27] X. Pan, H. Olesen, and B. Tromborg, Electron. Lett. **26**, 1074 (1990).
[28] D. Baums, Ph.D. thesis, Philipps—Universität Marburg, Germany (1990).
[29] P. Bak, T. Bohr, and M. H. Jensen, Phys. Scr. T **9**, 50 (1985).
[30] R. Adler, Proc. IRE **34**, 351 (1946).
[31] H. Haus and H. L. Dyckman, Int. J. Electron. **44**, 225 (1978).
[32] J. O'Gorman, B. J. Hawdon, J. Hegarty, and D. M. Heffernan, J. Appl. Phys. **66**, 57 (1989).
[33] S. Schuster, T. Wicht, and H. Haug, IEEE J. Quantum Electron. **QE-27**, 205 (1991).
[34] H. G. E. Hentschel and I. Procaccia, Physica **8D**, 435 (1983).
[35] H. Nakajima and R. Frey, Phys. Rev. Lett. **54**, 1798 (1985).
[36] R. Lang, IEEE J. Quantum Electron. **QE-18**, 976 (1982).
[37] R. Nietzke, P. Panknin, W. Elsässer, and E. O. Göbel, IEEE J. Quantum Electron. **QE-25**, 1399 (1989).
[38] R. Nietzke, P. Fenz, W. Elsässer, and F. O. Göbel, Appl. Phys. Lett. **51**, 1298 (1987).
[39] T. S. Parker and L. O. Chua, Proc. IEEE **75**, 982 (1987).
[40] P. Grassberger and I. Procaccia, Phys. Rev. Lett. **50**, 346 (1983); Physica **9D**, 189 (1983).
[41] Y. Termonia and Z. Alexandrowiez, Phys. Rev. Lett. **51**, 1265 (1983).
[42] C. Greborgi, E. Ott, and J. A. Yorke, Phys. Rev. Lett. **48**, 1507 (1982).
[43] We have experimentally determined the value for ϵ to be $\epsilon = 2 \times 10^{-18}$ cm^3 for this type of semiconductor laser.
[44] See, e.g., H. G. Schuster, *Deterministic Chaos* (Ref. [1]), p. 60.

[45] P. Glas, R. Müller, and G. Wallis, Opt. Commun. **68**, 133 (1988).
[46] Y. Cho and T. Umeda, Opt. Commun. **59**, 131 (1986).
[47] T. Mukai and K. Otsuka, Phys. Rev. Lett. **55**, 1711 (1985).
[48] J. Sacher, W. Elsässer, and E. O. Göbel, IEEE J. Quantum Electron. **QE-27**, 373 (1991).
[49] D. Lenstra, B. H. Verbeek, A. J. den Boef, IEEE J. Quantum Electron. **QE-21**, 674 (1985).
[50] N. Schunk and K. Petermann, IEEE J. Quantum Electron. **QE-24**, 1242 (1988).
[51] R. W. Tkach and A. R. Chraplyvy, J. Lightwave Technol. **LT-4**, 1655 (1986).
[52] B. Tromborg and J. Mørk, IEEE Photonics Technol. Lett. **PTL-2**, 549 (1990).
[53] B. Tromborg and J. Mørk, IEEE J. Quantum Electron. **QE-26**, 642 (1990).
[54] The output of the laser consists of an optical pulse train with each pulse separation equal to the cavity round-trip time $1/f_e$. Each of these pulses is followed by a weaker relaxation oscillation with a relaxation oscillation frequency of 3.8 GHz in this case. We attribute the broader peak in the power spectrum to a beat signal between the relaxation oscillation frequency and the pulse train frequency f_e.
[55] J. Mørk, B. Tromborg, and P. L. Christiansen, IEEE J. Quantum Electron. **QE-24**, 123 (1988).

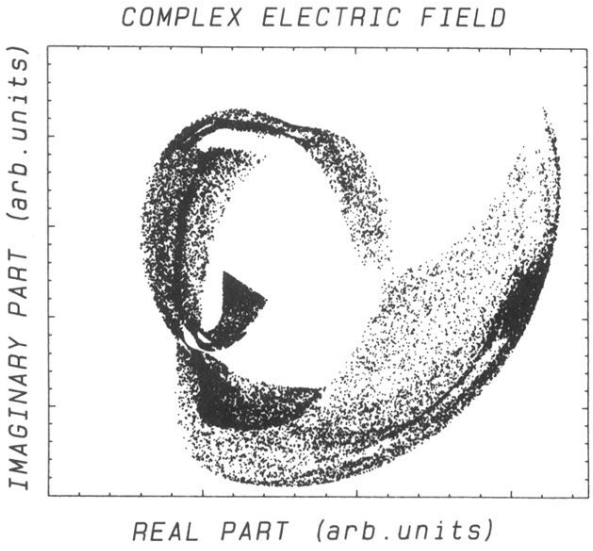

FIG. 8. Poincaré plot constructed from the simulated data as depicted in Fig. 7(e). Plotted are the intersection points of the trajectories for the plane of the complex electric field $\mathcal{E}$ defined by the transparency value N_{LD} of the carrier density.

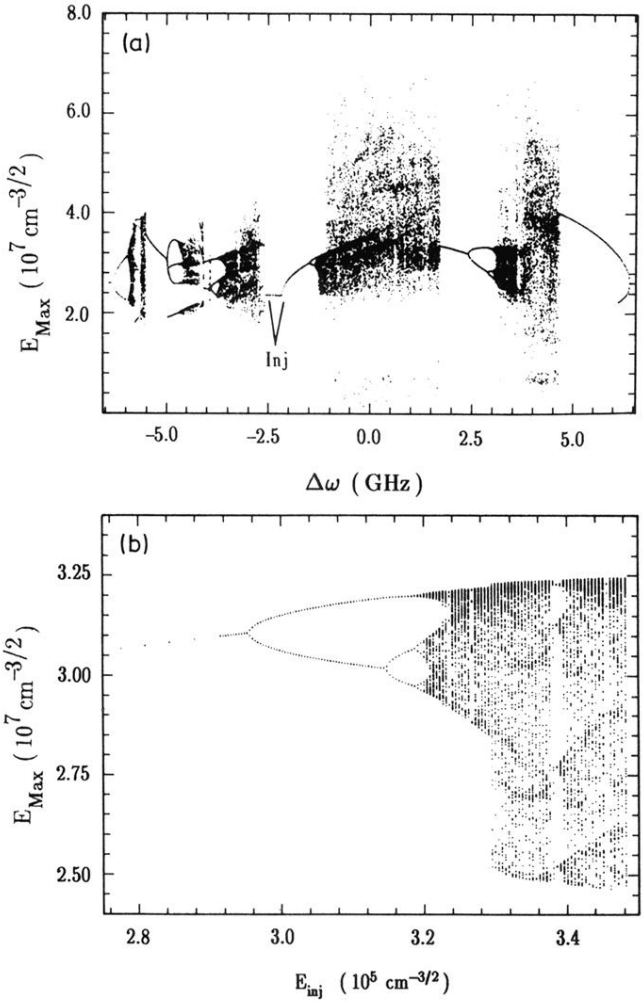

FIG. 9. Bifurcation diagrams with detuning frequency $\Delta\omega$ [(a) upper part] and the injected field amplitude E_{inj} [(b) lower part] as the control parameter, respectively. Plotted are the maxima of the electric field amplitude E occurring in the respective time trace. The locking range is indicated by inj. The values of α and ϵ are $\alpha=4$, $\epsilon=0$ cm^3.